University of Auckland
Department of Physics
Bachelor of Science, Physics and Chemistry

Photoacoustic Imaging & Flow Observation

Author:
Caitlin Smith

Supervisor:
Dr. Jami Shepherd

Abstract

In this experiment we aim to utilise the optical contrast of a blood mimicking media against tissue due to its strong absorption of light, and use this as a basis to perform photoacoustic (PA) experiments. PA waves are generated by the absorption of a pulse of light, which results in the emission of broadband ultrasound waves, that can be detected at the surface of a sample. Initially, these experiments were run on pencil lead embedded in phantom tissue, where a laser doppler vibrometer (LDV) was used to observe PA wave arrivals at a localised position on the surface. Then, different diameters of pencil lead were studied with this set-up and their differences observed through study of the PA arrivals and analysis in the frequency domain. The experimental set-up evolved to include a clinical ultrasound probe to image the different sizes of lead underwater. The cleanest image was reconstructed through optimisation of the speed of sound. Finally, ink was pumped through tubing to replicate blood flowing through a vessel. Images were reconstructed and the first steps were made toward quantifying the flow speed based on analysis of the frequency domain and Singular Value Decomposition to isolate the flow-signal.

Contents

1 Introduction

1.1 Report Format

Originally this report started off at 30 pages, which is a bit of a mission for whoever needs to read it. To slim things down all the experiments up to the Flow Section have been summarised to the introduction/method (overview) and the conclusion (findings). Any other parts the become relevant for the flow section have also been included. If you want to read the whole report I am happy to email it.

1.2 Photoacoustic Imaging

Photoacoustic (PA) imaging creates ultrasound (US) waves in a sample though excitation by temporally modulated (pulsed) light. In this report the term "PA waves" is used to describe the US waves generated by absorption of light. When light is specifically absorbed by certain anatomical features, it creates a small temperature rise (less than 0.1K). This produces an initial pressure increase which relaxes via emission of broadband low-amplitude acoustic waves [1]. These waves can then be detected at the surface of the sample and used to form an image.

PA imaging is only possible due to developments in laser technology that have occurred over the past few decades. The laser is a single frequency light source which enables specific components of a sample to be selectively excited by absorbing this light to emit US. Lasers are also able to deliver short yet powerful pulses of light, such that the duration of tissue excitation via laser light is practically instantaneous compared to the time taken for US waves to travel to the surface to be detected. A benefit of PA imaging is that pre-exisiting clinical ultrasound probes are able to be used for the detection of PA waves, making PA imaging a very feasible technique for use in a clinical setting soon.

PA imaging is a promising modality for functional studies of biological systems as it focuses on optical contrast instead of the acoustic impedance used in US imaging. Chromophores are the part of a molecule responsible for its color and are abundant in certain features of tissue. Some examples of optically active tissue components include haemoglobin, water and lipids [1].

2 Pencil Lead Phantoms-LDV

2.1 Overview

For this experiment we embedded a piece of pencil lead (0.7mm) in phantom tissue. The phantom tissue was made of 1g agar, 1mL intralipid and 200ml of water.
To record the PA arrivals a Polytech laser Doppler vibrometer (LDV) was used. This sends a laser beam with a single frequency onto the surface of the sample, which reflects back to the detector from retro-reflective tape sitting on its surface. As the sample's surface moves, the reflected beam will experience a frequency shift, which can be decoded to give the surface displacement as a function of time. A diagram of this set-up is shown in Figure 1. The sampling rate is 20M samples per second, meaning the greatest frequency we can observe is 10 MHz (Nyquist).

For the laser excitation, we used an Optical Parametric Oscillator (OPO) at 680nm which is absorbed by the lead [8]. The experiment was repeated 50 times, and the resulting PA waveforms from the LDV were averaged. The experiment was then repeated for 4 different lead diameters: 300, 500,700, 900 μm.

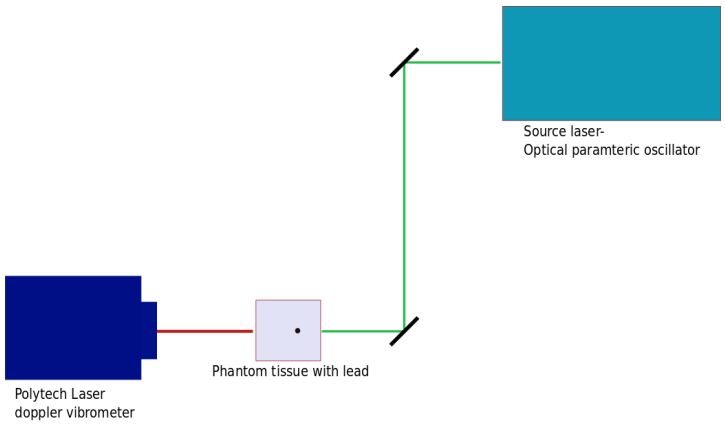

Figure 1: This diagram show a plan view of our set up for recording PA waves through the phantom tissue. Laser light is incident on the phantom from the OPO (optical parametric oscillator) using a series of mirrors. The vibration is detected on the opposite face by a LDV. The phantom is a cube of phantom jelly with a pencil lead standing vertically in it. There is a piece of retro-reflective tape on the face where the laser Doppler vibrometer beam hits the surface, to aid this beams reflection.

2.2 Findings

Using a single point ultrasound detector (LDV), a PA study of a pencil lead in phantom tissue was undertaken. Given the arrival of PA waves at the detector, seen in the top plot of Figure 2a, possible PA sources and paths within the phantom were determined. Unique peak frequencies for each of the different diameters of pencil lead could not be distinguished as the frequency spectra are not significantly different for each diameter of lead. This is shown in the bottom plot of Figure 2a. The signal observed at the face of the phantom will have a reduced high-frequency content due to attenuation that occurs between the lead to the detector. This means that the predicted peak widths will not correspond to a length equal to the diameters of the leads, however increases peak widths did correspond to an increase in lead diameter as seen in Figure 2b.

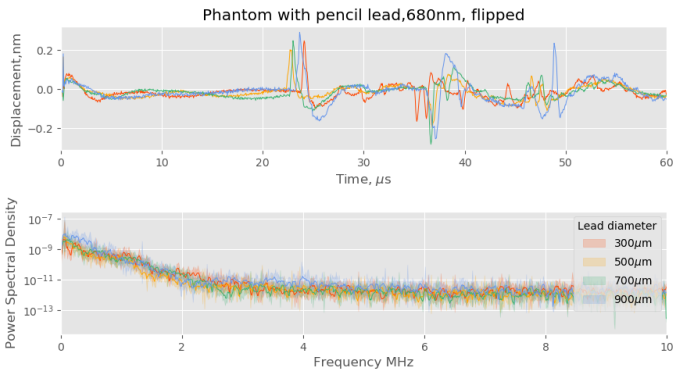

(a) The top plot shows the PA waveforms for each of the lead diameters. On the bottom is the power spectral density of the signals.

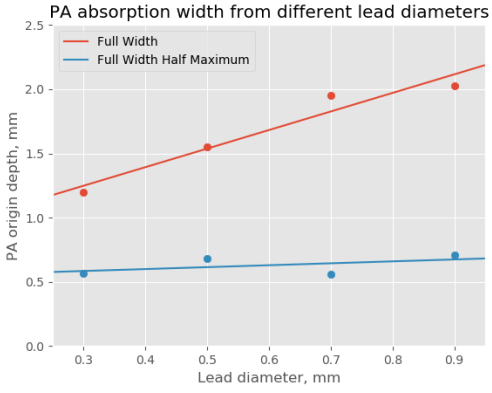

(b) This plot shows the full width and the full width at half-maximum of the PA signal that originated at the pencil lead against the lead diameter.

3 Imaging Pencil Leads with Verasonics

3.1 Overview

In this experiment, we aimed to move beyond a single PA detector to an array. For this we used a Verasonics clinical ultrasound probe to detect PA signals across the probe's 128 sensors. By having more sensors and knowing their spatial arrangement along the probe, images can now be reconstructed to create B-scans, using light to excite US waves generated at an optical absorber (pencil lead in the experiment). Once again we used the four different diameters of pencil lead with the intention to distinguish their size based on the images created.

Figure 3 shows the set up of this experiment. To create an image the, OPO was pulsed with a very small pulse duration (on the order of nanoseconds) with a repetition rate of 20 Hz. For each repetition the Verasonic probe recorded the arrivals of the PA signals, sampling at 31.25M samples per second, with 1280 samples taken per repetition. We attempted to take 50 records per pencil lead, however, due to a bug in the code, only one record per lead was taken, so no averaging of waveforms could occur. The laser trigger and data recording were performed using a script in Matlab.

3.1.1 Image reconstruction

Image reconstruction for data collected from the Verasonic system was undertaken in Matlab using the conventional delay-and-sum method. Initially the speed of sound (SOS) in the medium was defined as 1500m/s to get a basic image. Then different SOSs were tested to determine the SOS which created an image with the greatest quality. A mesh grid was created where the spatial arrangement of the sensors in the probe was on the x axis, and the depths probed were the y-axis. Then for every sensor position along the x-axis, Pythagoras is used to determine the distance from that sensor to each pixel. The delay is found by dividing this distance by the speed of sound. We then interpolated the signal data for this delay time for each pixel relative to that specific sensor. Each sensor's mesh is combined in a matrix which is resized to match the size of the image mesh. The envelope of this matrix is plotted to give our reconstructed image.

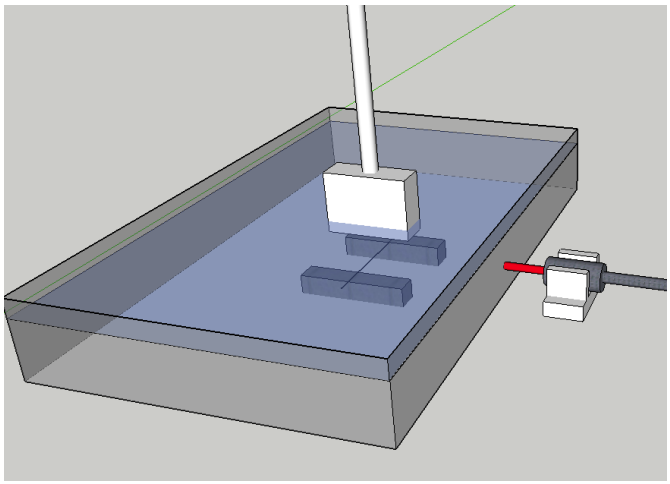

Figure 3: Table top set up for the PA experiment using the Verasonic system as the detector and different diameters of lead. The experiment took place in a large Pyrex dish filled with water. The lead sat between two supports on the bottom of the dish. The laser was manipulated into the side of the dish via an optical fibre, with a lens to focus the beam into this fibre near the OPO. The ultrasound probe sat above the dish with the probe tip submerged.

3.1.2 Speed of sound optimisation

In order to reconstruct the clearest images the SOS used in the data processing step above must be chosen correctly. To do this we used a

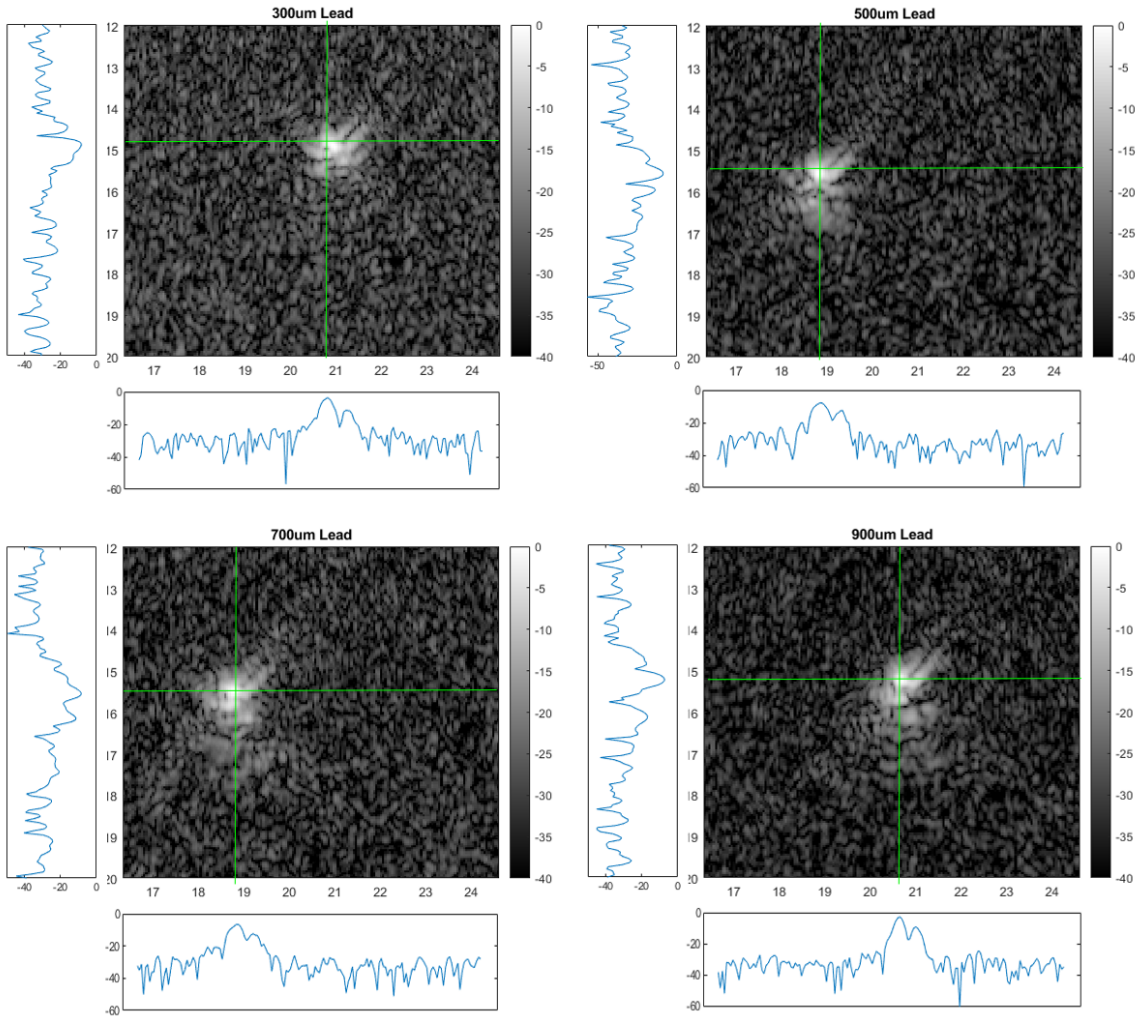

Figure 4: Image reconstruction for each of the different diameters of pencil lead. Vertical and horizontal cross sections through the centers are shown to display the image envelope through the centre of each lead. For these images, the speed of sound was set to 1507/s as determined by the focusing function method. Top L-R: 0.3mm, 0.5mm. Bottom L-R: 0.7mm and 0.9mm.

toolbox in Matlab called k-wave [9] and a script
called focusingfunctions.m [10]. This script creates a 3D stack of images (like pages in a book), where each "page" is an image created using one of the SOSs being trialled. The script determines how focused the image is at each SOS using a variety of focusing methods [9]. Each method in the focusing function is plotted to show how the different methods determine the focus for each speed of sound. These methods should converge on the SOS that gives the best image resolution and should match the true speed.

3.2 Findings

By introducing an ultrasound detector with 128 sensors, images could be reconstructed based on excitation of pencil leads with four different diameters using 680 nm light, as seen in Figure 4. The SOS used for the image reconstruction was optimised to give the most focused images.
The pencil lead is under-resolved in each image with a low SNR. The shapes of the leads are not

the crisp disks we would expect for cross-sections through pencil leads. These images are of poor quality because they were created from only one scan. If we were able to average 50 wavesforms to recreate this image, noise would be weaker. As a result the contrast between the lead signal and the surroundings would be higher leading to the creation of higher-contrast images. Furthermore, most of the detail that can be contained within a PA signal is the high frequency component, which attenuates quickly within the water before it reaches the detector, hence the equality of our images will never be perfect with this set-up.

4 Flow Sensing with Verasonic

4.1 Method

For this first flow measurement we tried to repeat the findings of Yao [12] by observing a Doppler shift in the frequency domain as the flow speed changed. In our experiment, our light signal will only be temporally modulated (pulsed) not spatially. To find the range of velocities to trialled in this experiment, the maximum velocity that could measured had to be determined. This was limited by the temporal separation between consecutive images formed, which was limited by the laser repetition rate and the Nyquist limit: $f_{max,Doppler} = f_{slowtime}/2$, [11], where $f_{slowtime}$ is our laser repetition rate. Now the Doppler shift for PA modulation is :

$$\Delta f = f_0 \frac{v_{flow}}{v_s} cos\theta$$

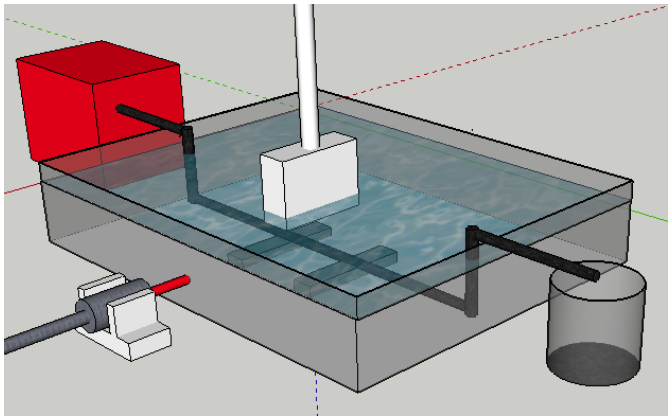

Figure 5: PA Flowmetry set-up. The red box is the pump which pushes a syringe full of ink through the tubing. The laser is shown on the left face of the glass pyrex dish, and the ultrasound probe is suspended into the water from above with the tip submerged.

Where Δf is the Doppler shift, f_0 is the transducer frequency, v_{flow} is the flow speed and v_s is the speed of sound in the medium. To find the maximum flow velocity, the maximum Doppler shift corresponds to $f_{max,Doppler}$ above. By equating the two equations and rearranging for v_{flow} with $\theta = 0$;

$$v_{flow,max} = \frac{\Delta f_{max}}{f_0} v_s = \frac{f_{slowtime}}{2f_0} v_s = \frac{20Hz \times 1500m/s}{2 \times 7.5 \times 10^6 Hz} = 2mm/s$$

Once the data was acquired, we reconstructed a series of images like frames of a movie, and picked one point in each of these images to observe as time progressed. The power spectral density of this signal would be obtained for each of the speeds used, and a shift in this signal due to changes in flow speed should be observed. The experimental set up is shown in Figure 5.

In this experiment we chose to look at 3 different flow speeds in the tube; 0mm/s, 1mm/s, and 2mm/s. For each of these speeds 1000 PA excitations were undertaken using the same laser parameters as in the previous section. The tubing used had an internal diameter of 3.175mm and an outer diameter of 4.775mm, while the ink in the tube is 100% India ink to ensure maximum

PA absorption.

To run the experiment, 1000 images at each flow speed and each orientation (perpendicular to probe and parallel to the probe, referred to as "longitudinal") were taken. To take an image, a short laser pulse is fired and the ultrasound probe's 128 sensors record the arrival of PA waves across the detector. 1280 samples are recorded within each repetition, with the same sampling frequency as in the previous Verasonics experiment. The laser repetition rate was 20Hz, so each flow speed and orientation took 50s seconds to record. Image reconstruction and SOS optimisation were undertaking in the same manner as in the previous Verasonics experiment. An optimum SOS of 1500m/s was used for all flow speeds and orientations. Only an optimum SOS could be found for the perpendicular orientation as the longitudinal focus increased with SOS beyond a physically possible value.

4.2 Sensor Data and Image Processing

In order to observe a Doppler shift, the sensor and image data for each frame can undergo several processes in an attempt to extract useful information. The raw data from the Verasonic system can undergo bandpass filtering and apodisation. The reconstructed image data can undergo Principal Component Analysis (PCA) or Single Value Decomposition (SVD) to distinguish between stationary and flowing regions [5].

- Bandpass Filter: removes frequency extremes. This has the effect of being able to remove high frequency noise which can clutter a signal to make the useful underlying signal more obvious. In the study done by Bucking [4], it was found that performing a high-pass filter was crucial to ensuring flow-speed was not overestimated when using a cross-correlation method for velocity mapping.

- Apodisation: a process used to smoothly bring a signal down to zero, minimising oscillations. As a result it is known as a tapering function and has the effect of reducing side lobes on signals at the expense of resolution. In this analysis, Hanning apodisation is used.

- Singular Value Decomposition (SVD): used to reject clutter in our images [5]. It utilises the different properties of our sample's components including spatio-temporal coherence (STC) to distinguish blood (ink) from tissue (water). If a pixel's STC is low (such that it varies greatly over the course of 1000 frames), it is attributed to noise, mid-range STC is attributed to blood flow and low STC is attributed to stationary tissue. Threshold singular values are defined to remove noise and possibly stationary signal, leaving behind image that corresponds to the region where flow occurs.

4.3 Results

4.3.1 Images

The images seen in Figure 6 do not show significant differences in image clarity between the different image processing methods used. For the perpendicular images, the apodisation process reduces the streaks (grating lobes to due to finite aperture), coming from tube. The band-pass filter makes the PA signal stronger and take up more space in the image. The combination of the bandpass filter and apodisation creates the best image, where streaks are minimised and the

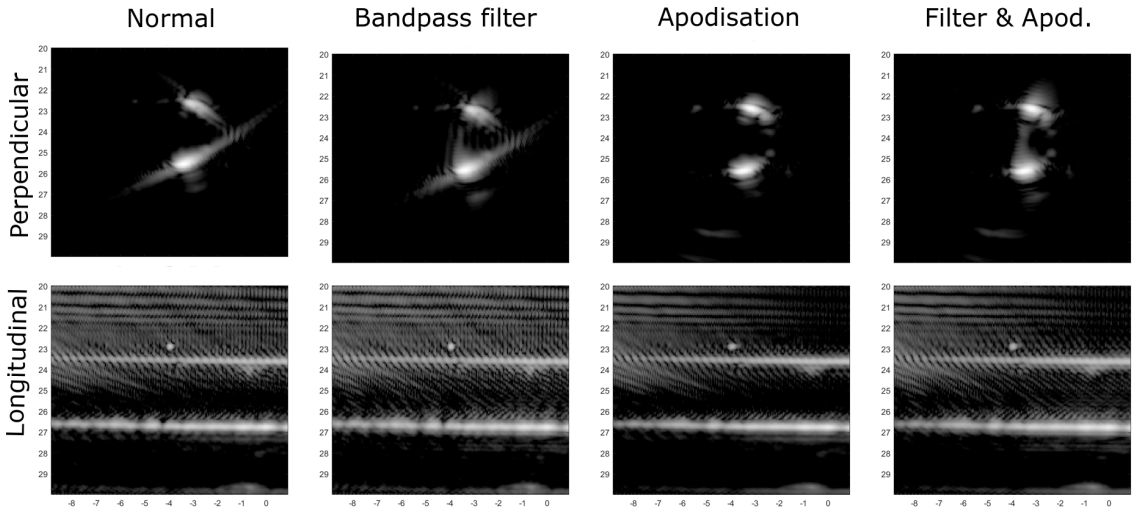

Figure 6: Above shows how the different image processing techniques changed the resulting image envelopes for both longitudinal and perpendicular images. All of these images are an average of the 1000 frames taken when the flow was stationary (V=0mm/s).

greatest area of the inner tube is illuminated. As for the longitudinal orientation, the difference between the images created is very small. The apodization process probably has the greatest effect on the image by decreasing artifacts above the tube, caused by PA reflections within the lens. However, this process is more effective at suppressing noise on the right hand side than the left. I suspect there was an air bubble on top near the centre of the tube as shown by the little white dot.

4.3.2 SVD

The SVD images are shown in Figure 7 for our band-pass filtered and apodised images, at the three different flow rates. Using a threshold value of $1 < \lambda_i < 5$, the images after SVD show a strong signal due to the PA emission, and have no streaking patterns or noise seen as in the images before. As we are only removing low value λs, we are only removing low STC noise signal. We do not see mid-range STC corresponding to flow due to a lack of heterogeneity in the blood mimicking fluid. Overall, this method was ineffective for observing flow, however it was able to separate signal from noise to make our PA images much clearer.

4.3.3 Frequency Investigation

Initially, we tried to observe a peak in the frequency spectrum for the sensor data (either raw, bandpass filtered, apodized, or both filtered and apodized), by observing a point in each frame's PA signal that originated at the tube. This point's evolution over all of the 1000 frames was observed by applying a Fast Fourier Transform to it. The FFT for all of the different types of sensor data showed no trends or significant peaks corresponding to a Doppler shift due to flow in the tube, hence none are shown in this report. We then tried to take the average value of a 5x5 pixel area for each frame in region of signal that originated in the tube but the resulting frequency spectrum was still noisy and had no significant peaks due to a Doppler shift.

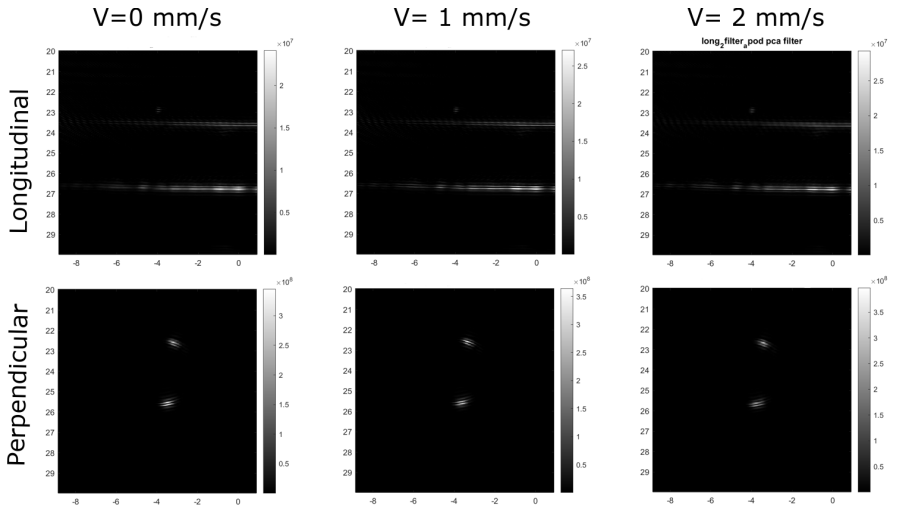

Figure 7: Images above show the image powers after SVD was performed on images that were previously bandpass filtered and apodised, at the 3 different flow speeds studied. We removed images with singular values greater than 5, as these have low STC so are attributed to noise. As we only have strong STC signal (ink) and weak STC, mid λ_i values that would be attributed to flow are not observed

For each of the flow speeds and image processing techniques used, the value of a pixel at a light and dark location on each reconstructed image was taken for each of its 1000 frames to create a signal. The light spot refers to a well-illuminated patch in the tube and the dark spot to a dark region where we would expect to see a PA signal from the tube. A Fast Fourier Transform was done on each of these signals in the hope of observing a peak at either 0Hz, 5Hz or 10 Hz, depending on whether the flow speed was 0mm/s, 1mm/s or 2mm/s respectively. Unfortunately no such trend was observed and all the frequency plots were random and noisy. Like before a 5x5 pixel area around the light and dark pixels chosen before were averaged for each of the 1000 frames and the frequency spectrum observed. This still had the same noisy signal with no prominent peaks due to a Doppler shift. The same was also done for the SVD images with the same outcome.

4.4 Discussion

In Figures 8a and 8b, the true tube dimension have been superimposed over the top of the images to show what the PA images are representing. The perpendicular image shows that the PA absorption is much stronger on the right side of the tube, which faced the incoming laser light. As a result, the left side isn't well-illuminated, so it doesn't emit PA waves, hence why it appears dark on the reconstructed images. This image confirms that most of the light is absorbed by the ink in the tube and not by the tube itself, which means the tube is effectively invisible in this study. Another reason why the far side of the tube was dark may be that the tube was too wide and the ink too absorbing to allow light to pass to the other side. As for the longitudinal images, the tube shape is a more realistic than in the perpendicular ones. There are a large number of artifacts observed above the tube which are likely to be reflections generated in the lens.

Ultimately we were unable to determine the speed of the fluid in the tube via PA imaging. This due to the homogeneity of the India ink at this resolution as a result of the tiny size of the carbon colloids in the ink. Even if we were able to observe the flow, we would tend to under-measure the flow speed as most of the PA absorption occurs near the sides of the tube where the flow is slowest due to friction with the tube walls. This neglects the fastest part of the tube, so that the signal

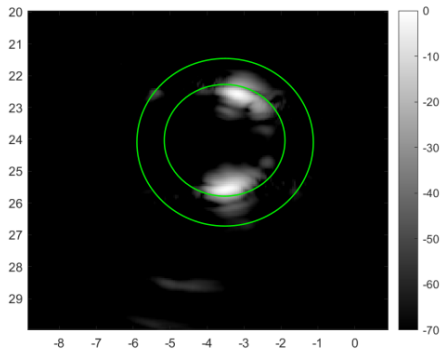

(a) In the diagram above, the perpendicular image with the bandpass filter applied is shown with the true tube dimensions superimposed over the top. The inner circle marks the internal diameter and the outer ring the external diameter.

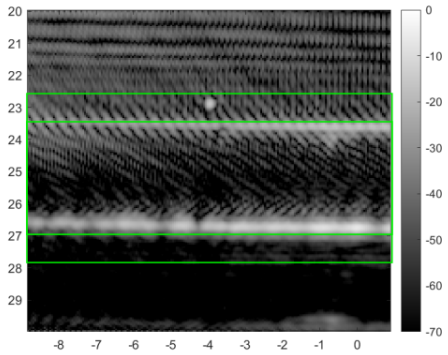

(b) In the diagram above, the longitudinal image with the bandpass filter applied is shown with the true tube dimensions superimposed over the top. The inner box marks the internal diameter and the outer box is the external diameter.

Figure 8: The pictures above show the reconstructed images with the true tube dimensions superimposed over the top

observed would only be from the slowest flow regions and not representative of the average flow.

4.4.1 Improvements

To achieve PA emission from the middle of the tube to observe a more complete image we could dilute the ink so light can penetrate deeper before being absorbed and use a thinner tube. To get a signal from the whole tube, a diffuser could be added to spread the light, so it is absorbed from all sides, evenly emitting PA waves for more accurate image reconstruction. To improve image quality, speckle patterns could be added [7]. This can be done dynamically by adding a rotating speckle disk [6] in front of the laser. Speckle is invaluable in US imaging, however PA imaging is speckle-free as imaging results from optical absorption contrast [7]. The reason we could not observe flow in our images is that our fluid was homogeneous, due to the small size of the ink particles. Heterogeneity can introduced by adding relatively large polystyrene particles [3], [2] to extract a PA signal with a strong enough Doppler shift to be observed using the FFT and SVD methods. This will have the advantage of better replicating red blood cells, which is ideal as eventually we hope to use this technique for real-world medical applications. We could also use a different method to observe flow. Cross-correlation (CC) between subsequent frame's tube signal region is used to find an average lag time, which can be used to work out the flow [3], [2], [4]. Finally to observe a wider range of physically relevant flow speeds, a laser with a higher repetition rate or an US probe with a lower center frequency could be used.

4.5 Conclusion

By using our 128 sensor ultrasound probe and applying a variety of data processing techniques, the image clarity was increased for both the perpendicular and longitudinal orientations. The flow speed was unable to be determined as no Doppler shift could be observed in any of the frequency spectra for both the data and the images across the 1000 frames taken in each experiment. SVD was also unable to correctly attribute image regions to their flow speed and showed no change

with varying flow speeds. For this experiment the India ink was effectively homogeneous so no flow could be detected as the particles that make up the ink are too small and the fluid too dense.

4.6 Acknowledgements

Huge thanks must go to Jami for all her guidance and expertise in this project and Neil at the Photon Factory for this opportunity. I can't wait to continue this work with you all!

References

[1] Paul Beard. Biomedical photoacoustic imaging. *Interface Focus*, 1(4):602–631, August 2011.

[2] Joanna Brunker and Paul Beard. Pulsed photoacoustic Doppler flowmetry using time-domain cross-correlation: Accuracy, resolution and scalability. *The Journal of the Acoustical Society of America*, 132(3):1780–1791, September 2012.

[3] Joanna Brunker and Paul Beard. Acoustic resolution photoacoustic Doppler velocimetry in blood-mimicking fluids. *Scientific Reports*, 6(1):20902, February 2016.

[4] Thore M. Bücking, Pim J. van den Berg, and Stavroula Balabani. Processing methods for photoacoustic Doppler flowmetry with a clinical ultrasound scanner. *Journal of Biomedical Optics*, 23(02):1, February 2018.

[5] Charlie Demené, Thomas Deffieux, Mathieu Pernot, Bruno-Félix Osmanski, Valérie Biran, Jean-Luc Gennisson, Lim-Anna Sieu, Antoine Bergel, Stephanie Franqui, Jean-Michel Correas, et al. Spatiotemporal clutter filtering of ultrafast ultrasound data highly increases doppler and fultrasound sensitivity. *IEEE transactions on medical imaging*, 34(11):2271–2285, 2015.

[6] Jérôme Gateau, Thomas Chaigne, Ori Katz, Sylvain Gigan, and Emmanuel Bossy. Improving visibility in photoacoustic imaging using dynamic speckle illumination. *Optics letters*, 38(23):5188–5191, 2013.

[7] Zijian Guo, Li Li, and Lihong V Wang. On the speckle-free nature of photoacoustic tomography. *Medical physics*, 36(9Part1):4084–4088, 2009.

[8] Jami L. Johnson, Mervyn Merrilees, Jeffrey Shragge, and Kasper van Wijk. All-optical extravascular laser-ultrasound and photoacoustic imaging of calcified atherosclerotic plaque in excised carotid artery. *Photoacoustics*, 9:62–72, March 2018.

[9] Bradley E Treeby and Benjamin T Cox. k-wave: Matlab toolbox for the simulation and reconstruction of photoacoustic wave fields. *Journal of biomedical optics*, 15(2):021314, 2010.

[10] Bradley E. Treeby, Trond K. Varslot, Edward Z. Zhang, Jan G. Laufer, and Paul C. Beard. Automatic sound speed selection in photoacoustic image reconstruction using an autofocus approach. *Journal of Biomedical Optics*, 16(9):090501, 2011.

[11] P.J. van den Berg, K. Daoudi, and W. Steenbergen. Review of photoacoustic flow imaging: its current state and its promises. *Photoacoustics*, 3(3):89–99, September 2015.

[12] Junjie Yao, Rebecca C. Gilson, Konstantin I. Maslov, Lidai Wang, and Lihong V. Wang. Calibration-free structured-illumination photoacoustic flowgraphy of transverse flow in scattering media. *Journal of Biomedical Optics*, 19(4):046007, April 2014.